Available online at www.sciencedirect.com

ScienceDirect

Procedia CIRP 58 (2017) 104 – 109

www.elsevier.com/locate/procedia

16th CIRP Conference on Modelling of Machining Operations

Kinematic hardening of AISI 5120 during machining operations

Andreas Fellmeth[a]*, Frederik Zanger[a], Volker Schulze[a]

[a]*wbk – Institute of Production Science, Karlsruhe Institute of Technology (KIT), Engelbert-Arnold-Straße 8, 76131 Karlsruhe, Germany*
* Corresponding author. Tel.: +49 721 608-46316; fax: +49 721 608-45004. *E-mail address:* andreas.fellmeth@kit.edu

Abstract

Metal manufacturing processes like machining include complicated load cases and significant plastic deformation inside the manufactured component. The Finite-Element-Method (FEM) has been successfully applied to analyze machining processes.
The plastic deformations during machining operations, especially of ductile materials, are a major part of the total deformation. If the deformation incorporates a large plastic deformation part with changing spatial directions, kinematic hardening should be considered, additionally to isotropic hardening. Previous work on the kinematic hardening of ARMCO iron revealed an almost near constant ratio of isotropic and kinematic hardening. The constant kinematic hardening ratio is revised and analyzed in tensile-compression tests with normalized AISI 5120. The FEM simulation results using the new material model of the kinematically hardening AISI 5120 are validated with experimental force measurement during orthogonal machining. The influence of kinematic hardening during machining operations is not the major influence, but still substantial.

Peer-review under responsibility of the scientific committee of The 16th CIRP Conference on Modelling of Machining Operations

Keywords: Finite element method (FEM), Machining, Kinematic hardening

1. Introduction

Machining operations include complicated load cases inside the manufactured component. The FEM has been applied to analyze the machining process, and characteristics like temperature, residual stresses and process forces.

Machining operations are very hard to simplify, considering the large amount of interdependencies between the thermo-mechanical variables calculated within the analysis. Usually, plastic deformation heats up the material, which results in changing temperatures, which themselves change the material properties. Most engineering simulations only incorporate isotropic hardening, because it is both easier to implement and to test for, and usually the more dominant material behavior compared to kinematic hardening. Kinematic hardening is however an important effect [1,2], depending on the degree of simplification and abstraction.

Fig. 1 shows the basic concept of kinematic hardening and its effect on the movement of the yield surface. In contrast to isotropic hardening, the yield surface keeps its initial size

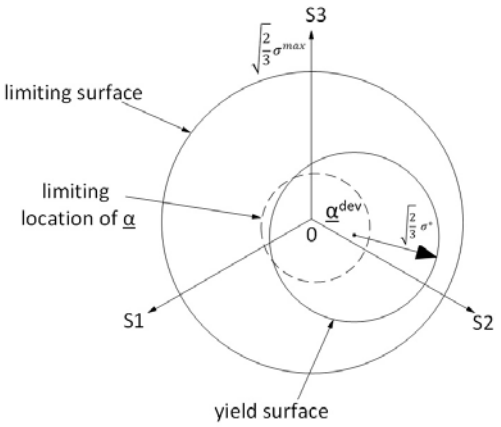

Fig. 1 Kinematic hardening in the stress space [3]

Peer-review under responsibility of the scientific committee of The 16th CIRP Conference on Modelling of Machining Operations
doi:10.1016/j.procir.2017.03.201

during pure kinematic hardening. Fig. 1 also shows a bounding limit to the amount of kinematic hardening, which is contained within a cylinder, due to the Mises yield stress definition, as described in the ABAQUS documentation [3].

Groundwork in the field of kinematic hardening was published by Armstrong and Frederik [4]. The application to viscoplasticity was done by Malinin and Khadjinsky [2,5]. To apply this work to modern FEM, additional problems had to be solved.

Notably Simo and Taylor published about the importance of consistent tangent operators when using a nonlinear 'incremental' model [6]. This tangent operator makes the quadratic convergence of solutions possible, gained by the iterative Newton method [7]. The use of the 'normal' elastic tangent modulus would not result in optimal convergence, but still give the same result. The constitutive equations derived describe J_2 plasticity in this work.

Because of the details of the implementation, a strain rate and temperature dependent kinematic hardening model is not stable with a fully thermo-mechanically coupled FEM simulation subjected to large nonlinear material deformations. For highly non-linear problems, as in thermo-mechanical numerical calculations, the combined isotropic-kinematic-hardening routine may trigger convergence problems [3, 12]. These might arise due to convergence issues during the Newton algorithm, which is implemented to solve the material equations during FE-analysis. This would eliminate the possibility to find a solution using an acceptable time increment. Small models, with small deformations, subjected to moderate temperature changes can be calculated using a custom UMAT subroutine, following the implementation introduced by Simo and Taylor [6]. This UMAT allows complete freedom in material model implementation, and allows for the implementation of a consistent tangent modulus. As for the intrinsic software possibilities, the calculation of kinematic hardening combined with any changing thermal simulation component using the proprietary functions within ABAQUS is prohibited by the software itself.

The kinematic hardening model is therefore implemented in the ABAQUS 'combined kinematic hardening'-model, which can include thermal dependencies (at different isothermal states) and strain rate dependencies (the strain rate dependencies can be used directly within the model, if the deformation produces different strain rates within the geometry).

With those limitations at hand, the influence of kinematic hardening on the cutting simulation is analyzed, the question being: How large is the influence of kinematic hardening if used in a simulation model on the simulation results, compared to a simulation model with isotropic hardening only, and compared to a simulation model with different constant friction parameters.

Nomenclature

γ	Scalar value (zeroth order tensor, small letters)
$\boldsymbol{a}$	First order tensor (bold small latin letters)
$\boldsymbol{\sigma}$	Second order tensor (bold small greek letters)
$\boldsymbol{C}$	Fourth order tensor (bold capital letters)

1.1. Preliminary remarks

Zanger et al. [8] used a constant linear kinematic hardening ratio, called Bauschinger-effect-parameter, which was originally mentioned in the work of Ibrahim and Embury [9] and which is constant in the range of the total equivalent plastic strain.

The ratio used to describe the experimental findings in this work is different compared to Zanger et al. [8]. A more detailed material model of normalized AISI 5120 was used, compared to the normalized ARMCO iron in the previous work.

In this paper, first, the hardening data and methods are established while explaining the choices made. Then the experimental results are being described and compared to the simulation. A closing discussion follows. Closing remarks are then made on further need for research on this topic.

2. Experiments and simulation methods

2.1. Kinematic hardening characterization and experimental results

To determine material parameters related to kinematic hardening in the specific material AISI 5120 (normalized), experimental work was necessary.

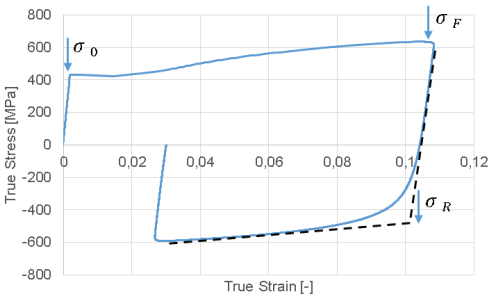

Fig. 2 True strain - true stress measurement, tensile-compression, at room temperature (approx. 293 K), force regulated, low strain rate. Material AISI 5120.

The results to implement the movement of the yield surface in the stress space were quantified by dividing the difference of the maximum stress in the primary load direction σ_F and the second opposite load direction σ_R by σ_F, see equation (1). The values used are visualized in Fig. 2. As the movement of the yield surface consists of only half the ratio, the ratio needs to be divided by 2. The resulting ratio is called r_{imp} ("ratio for implementation").

$$r_{\mathrm{imp}} = \frac{\sigma_F - \sigma_R}{2 \cdot \sigma_F} \tag{1}$$

This quotient r_{imp} will directly be used to accordingly modify the isotropic hardening material model data.

Ibrahim and Embury [9] used another ratio which implicitly contained information about kinematic hardening. The ratio in equation (1) only has this information as long as the total yield stress for all relevant plastic strain is also known in an additional equation or tabular data. This is the case in this work.

The values measured for the tensile-compression and compression tensile tests were carried out with strain-gauge and machine position values for the strains. As the tests were done force controlled, the total strain experienced by each specimen varies. Also, in some tests the yield strength could not be clearly determined. Since the strain-gauge and the machine position were not giving the exact strain within the plastically deforming part of the specimen, this also contributes to further inaccuracies, and to a wider standard deviation of the results. To circumvent this inaccuracies, the value taken at a plastic strain of ε_{pl} = 0.02 was the arithmetic mean of a small group of selected tests with a small standard deviation of +/-0.0177 due to clear elastic-plastic transition determined, resulting in a ratio of $r_{\mathrm{imp}} = 0.181$. The final total value of the ratio r_{imp} at highest plastic strains was set to 0.20 at ε_{pl} = 10. This constant value was chosen because the material science theories behind the effect of kinematic hardening forecast, that the kinematic hardening saturates at higher plastic strains, and remains fairly constant after that, if using other metals as Troiano et al. [10]. This is assumed as an upper bound of r_{imp} parameters. Additionally, a kinematic hardening simulation with the arithmetic mean minus standard deviation,$r_{\mathrm{imp}} = 0.164$ at ε_{pl} = 0.02 and a ratio of 0.10 at a plastic strain of ε_{pl} = 10, which is exactly 50 % of the value chosen at the previous parameters was performed. This serves as a lower bound, which probably underestimates the influence of kinematic hardening.

2.2. Experiments to validate the simulation results

For the experiments, a vertical broaching machine from Karl Klink with a maximum cutting speed of $v_{c,max}$ = 160 m/min was used. The length of the workpiece, a normalized sample of AISI 5120, is l = 80 mm, the width w = 20 mm and thickness t = 4 mm. A cutting tool with a cutting radius r_β = 40 µm, rake angle γ = -5° and clearance angle α = 5° was used. The process forces were measured by a Kistler three component dynamometer Type Z 3393. The cutting depth is h = 50 µm and the cutting velocity v_c = 1 m/min.

The processed surface shows traces of a non-stationary process (Fig. 3), with a built-up edge in front of the tool and spontaneous debonding from the remaining workpiece. However, the first millimeters of the surface show a relatively smooth finish, which is the cutting range covered in the simulations.

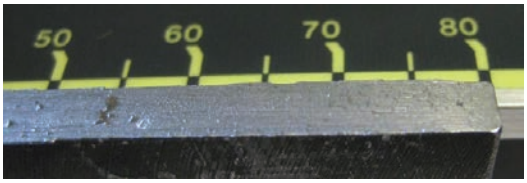

Fig. 3 Machined surface at low speed, smooth surface in the beginning part on the right, hardness testing indentation visible, scale with unit [mm]

2.3. 2D machining Simulation

During the computation of the 2D-machining simulation, true strains are applied in the computation, and all stress and strain tensors are rotated to account for rigid body motion.

A FE-model simplifying the real chip formation situation was run with the material parameters. The FE model handles an orthogonal cutting simulation with a continuous remeshing loop after a certain workpiece movement. Elements used are CPE3T and CPE4T. The cutting direction is parallel to the lower workpiece edge, giving a constant feed rate. The tool was assumed rigid. As can be seen in the work of Zemzemi et al. [11], a friction value of 0.35 is an overall acceptable approximation for machining simulations, and was used as an input value for friction in the simulations. For comparison a reduced value of 0.1 was also applied. A resulting banded contour plot from the ABAQUS-viewer is shown in Fig. 4, showing the temperature distribution [K] in the entire model.

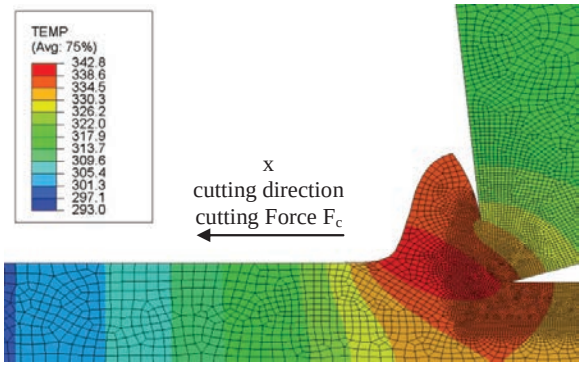

Fig. 4 2D machining simulation, cutting speed 1 m/min, cutting depth 50 µm, cutting edge radius 40 µm, friction coefficient 0.1

The chip formation is due to plastic deformation, i.e. no element separation was introduced in this simulation. The question how much of the chip formation motion is due to plastic deformation around the cutting tool and how much is due to material failure, is not being analyzed here. Excessive element distortion is countered by remeshing the workpiece. The remeshing is triggered at equal displacement intervals of the tool, the basic simulation details apply as for example published by Schulze et al. [12,13].

Table 1 Material parameters for AISI 5120 in normalized state, as stated by Schulze et al. [13]

Thermal conductivity		λ [W/(m · K)]	50
Thermal expansion		α_{th}[1/K]	1.15E-05
Heat capacity		c_p [J/(kg·K)]	460
Density		ρ [g/cm³]	7.85
Taylor–Quinney coefficient		η	0.9
Thermal flow stress part			
σ_0^* [MPa]	1885	$\dot{\varepsilon}_0$ [1/s]	1.01E07
m	1.78	ΔG_0	1.03E-19
n	0.5	k_b	1.38E-23
σ_{G0} [MPa]	400	σ_1 [MPa]	339
θ_0 [MPa]	5.56	θ_1 [MPa]	200
E [MPa]	2.1E05	υ	0.283

$$\sigma_F = \sigma_0^* \left(1 - \left(\frac{T}{T_0}\right)^n\right)^m + \left(\sigma_{G0} + (\sigma_1 + \theta_1 \varepsilon_{pl})\left(1 - \exp\left(-\frac{\theta_1 \varepsilon_{pl}}{\theta_0}\right)\right)\right)\frac{G(T)}{G(0\mathrm{K})} g \qquad (2)$$

with $T_0 = \frac{\Delta G_0}{k_B \ln\left(\frac{\dot{\varepsilon}_0}{\dot{\varepsilon}_{pl}}\right)}$

A material model of normalized AISI 5120 is used, based on the material model parameters used by Schulze et al. [13] and the equations, which are explained in detail by Weber et al. [14]. Equation (2) shows the model for the yield stress, which is later interpolated linearly.

Here g is a function only relevant to high temperature softening. Young's modulus was entered as temperature dependent tabular data, which is based on a fit function that can also be found in Weber et al. [13].

To incorporate the kinematic hardening, disabling the entire thermo-mechanical coupling within the simulation is necessary. The overall effect being, that the initially set temperature cannot change. In this isothermal situation, the Taylor–Quinney coefficient, heat generated by friction and all effects that would be triggered by a resulting change in temperature are not happening in this model. To quickly switch between purely isotropic hardening and combined isotropic-kinematic-hardening implementations, a tabular input for the combined isotropic-kinematic-hardening model in ABAQUS was chosen. This makes a stepwise linear interpolation of the material model, described in Schulze et al. [13], necessary. To judge if all these necessary alterations from the usual thermo-mechanical implementation result in an error too large in the cutting force, a direct comparison was performed. To further enhance the accuracy of the stepwise linear interpolated material, the model data uses non-equally-spaced intervals. Fig. 5 shows that a difference between the used models exists. However, the difference is acceptable and it is feasible to use this model for further analysis.

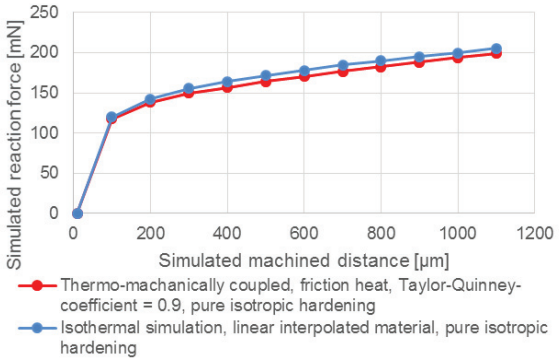

Fig. 5 Comparison between reaction force in cutting direction, with and without thermal information at cutting speed 1 m/min

Up to this point, the implementation was made possible, but the implementation details of kinematic hardening themselves were not discussed in detail. The kinematic hardening model is therefore implemented in the ABAQUS 'combined kinematic hardening'-model, which can include thermal dependencies at different isothermal states, but not within the simulation once it has started, since thermo-mechanical coupling has to be disabled. Strain rate dependencies can be used directly within the model, if the deformation produces different strain rates within the geometry.

The general relation for total yield stress is given in equation (3).

$$\boldsymbol{\sigma}_{yield}(\boldsymbol{\varepsilon}_{pl}) = \boldsymbol{\sigma}_{isotropic}(\boldsymbol{\varepsilon}_{pl}) + \boldsymbol{\alpha}_{kin}(\boldsymbol{\varepsilon}_{pl}) \qquad (3)$$

With bold greek symbols being tensors, $\boldsymbol{\sigma}$ the Cauchy stress and $\boldsymbol{\alpha}_{kin}$ the kinematic hardening backstress which are both monotonically increasing with the plastic strain $\boldsymbol{\varepsilon}_{pl}$ accumulated, $\boldsymbol{\alpha}_{kin}$ starting with Zero for $\boldsymbol{\varepsilon}_{pl} = 0$. The kinematic hardening calculation rule is included within ABAQUS (given here as scalar value) [3] as in equation (4).

$$\alpha_{kin} = \frac{C_K}{g_K}\left(1 - e^{-g_K \varepsilon_{pl}}\right) \qquad (4)$$

To find the correct values with the experiments done here, the quotient C_k/g_k is first renamed to A, which is the final value α_{kin} for $\varepsilon_{pl} \to \infty$.

$$\frac{C_k}{g_k} = A \qquad (5)$$

To determine the values of A and g_k, the total yield stress needs to be split up into kinematic hardening and isotropic hardening, the kinematic hardening material data input in ABAQUS is defined using the back-stress in equation (4) for largest strains. It is

$$A = r_{imp} \cdot \sigma_F$$

Related to r_{imp} = 0.2 (high boundary) and 0.1 (50 %) (low boundary) at $\varepsilon_{pl} = 10$ and the total yield stress at $\varepsilon_{pl} = 10$ being σ_F = 2.5 GPa, calculated from the material data given in Table 1 and equation (2) it is:

A = 0.5 GPa (high boundary) and A = 0.25 GPa (low boundary). This can be assumed because there will be almost no change of α_{kin} at higher values of ε_{pl} expected here.

Equation (4) has then been used to determine the value of g_k, using the only remaining unknown values at the small strain $\varepsilon_{pl} = 0.02$, r_{imp}= 0.181 and r_{imp} = 0.164, respectively.

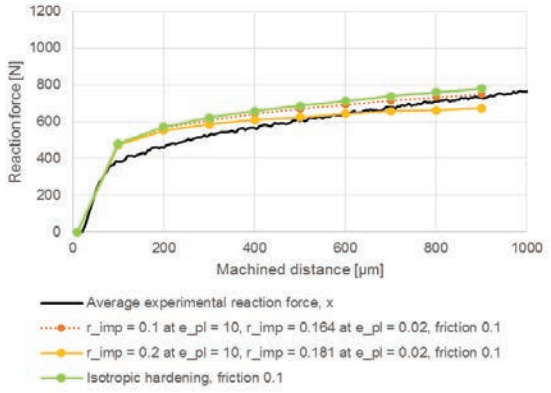

Fig. 6 Simulation with different kinematic hardening parameters, machining simulation and experiment, friction 0.1, kinematic hardening given with specific values of r_{imp} at exact strains ε_{pl}. Cutting speed 1 m/min.

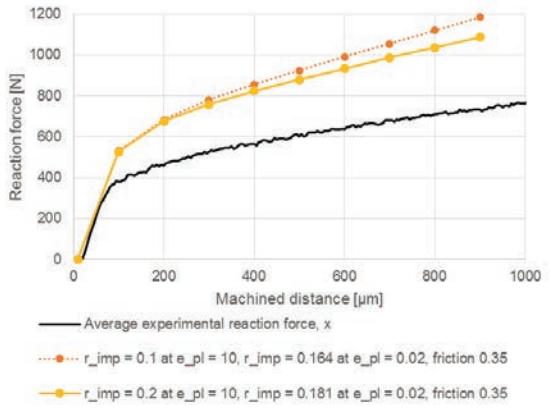

Fig. 7 Simulation with different kinematic hardening parameters, machining simulation and experiment, friction 0.35, kinematic hardening given with specific values of r_{imp} at exact strains ε_{pl}. Cutting speed 1 m/min.

$$\alpha_{kin} = r_{imp} \cdot \sigma_F$$

$$g_k = -\frac{\ln\left(1 - \frac{\alpha_{kin}}{A}\right)}{\varepsilon_{pl}}$$

This results in g_k = 10 (high boundary) and g_k = 20 (low boundary), if the parameters temperature T = 293 K and plastic strain rate $\dot{\varepsilon}_{pl}$ = 0 are used to calculate σ_F according to equation (2) and Table 1.

3. Results

Fig. 6 and Fig. 7 show the reaction force progress in the experimental setting, and resulting from the 2D-machining ABAQUS-simulation. The reaction force is also known as cutting force. The cutting forces shown use a friction value of 0.1 and 0.35 and the average experimental data gathered at the vertical broaching machine.

Simulation results of different kinematic hardening parameters, as described in Fig. 6, show a reduction of the reaction force depending on the kind of absolute kinematic hardening parameters. The results of the reaction forces using the lower bound hardening parameters $r_{\mathrm{imp}} = 0.164$ at ε_{pl} = 0.02 and $r_{\mathrm{imp}} = 0.1$ at ε_{pl} = 10 (dotted line) as well as the upper bound parameters $r_{\mathrm{imp}} = 0.181$ at ε_{pl} = 0.02 and $r_{\mathrm{imp}} = 0.2$ at ε_{pl} = 10 (yellow line) can be seen in Fig. 6. The average cutting force measured from experimental testing at the same cutting speed is also shown. Using isotropic hardening in the simulation produces the highest reaction forces.

Fig. 7 shows a similar setup as Fig. 6, with a friction coefficient of 0.35. Again, the same average cutting force measured from experimental testing and the same cutting speed is shown. The higher friction coefficient used in the simulation elevates the reaction forces by about 50 %.

4. Discussion

Ibrahim and Embury [9] found similarly constant values for kinematic hardening in ARMCO iron with a spread of roughly 30 % for ARMCO iron, but a different total value. A direct comparison of the values is not feasible, because the ratio describing kinematic hardening in the work of Ibrahim and Embury [9] differs from the ratio r_{imp} used in this work for AISI 5120, see equation (1), used here. However, qualitatively, it can be said that the kinematic hardening values found in the experiments in this work are higher, if compared to the values published by Ibrahim and Embury [9], no matter which quotient is calculated, because the values measured by Ibrahim and Embury [9] are smaller than the experimental values found in this work with equation (1).

Deducing from the experimental results, the kinematic hardening parameters presented in Fig. 6 show likely parameter boundaries, the highest estimate for upper bound kinematic hardening parameters (yellow line) suggests, that the kinematic hardening α_{kin} at 10 strain, amounts to roughly 0.5 GPa which seems to be a suggested extrapolation which

likely overestimates the real value. But even with this probably overestimated value, the total spread of cutting forces between isotropic and combined isotropic-kinematic hardening simulation results in Fig. 6 and Fig. 7 is still small. Comparing the different friction results of the simulations with the experimental values, Fig. 7 shows that the cutting forces resulting from the simulations with constant friction value of 0.35 are much higher than those reaction forces calculated with the constant friction value 0.1.

The well-fitting cutting force results in Fig. 6 show, that only small changes occur due to the possible range of feasible kinematic hardening parameters in the simulation results. A much larger change occurs, when changing the friction within the model. The chosen friction value of 0.35 is raising the cutting forces by about 50 % in the simulation results. This discrepancy in resulting influence between kinematic hardening and friction makes it clear, that the influence of kinematic hardening can clearly be shown even in complex macroscopic processes like machining simulations – however other parameter variations have a stronger influence on the result, within their possible parameter range, like the friction coefficient.

The implementation problem of kinematic hardening in fully coupled thermo-mechanical simulations only works on small simulation models with limited element size and deformation, using the FE-program ABAQUS. More results might be possible with an alternate FE-program, using different solver implementations within the software, which make kinematic hardening within a fully thermo-mechanical framework possible.

For more accurate predictions of the influence of kinematic hardening, the next step would be to measure the tensile-compression and compression-tensile behavior at higher accumulated plastic strain. As an inhibition, at those strains, strain-gauge measurements are difficult, and the stability of the testing sample for the second, inverted strain period (e.g. compression after elongation, or elongation after compression) becomes more and more an issue. Premature material failure might be the result.

5. Conclusion

A ratio was calculated from experiments, which were done to measure kinematic hardening using the Material AISI 5120. Parameters were set, due to this ratio, to run 2D-machining simulations. Due to numerical instabilities, a non-thermal, mechanical simulation had to be run. The kinematic hardening has a clear impact on the reaction forces measured at the vertical broaching machine, but this influence is smaller than varying the friction from a constant value of 0.1 to 0.35 in the entire 2D-machining simulation. The influence of kinematic hardening on the reaction forces shows roughly the same percentage as the kinematic hardening ratio within the implemented material model, given here as r_{imp}, or an even slightly smaller influence (e.g. $r_{imp} = 20\,\%$ leads to 15 % to 20 % lower reaction forces compared to the pure isotropic hardening case). Implementing the kinematic hardening in a machining simulation therefore remains a cost-benefit analysis: Only highly accurate machining simulations can benefit from this kind of material property implementation.

Acknowledgements

The authors are grateful for the project's funding by DFG within the research training group 1483 and computational resources provided at computation clusters IC2 and HC3 at KIT. Many thanks to the technicians at IAM – Institute for Applied Materials who helped with the experimental work.

[1] Hosseini E, Holdsworth SR, Kühn I, Mazza E. Temperature dependent representation for Chaboche kinematic hardening model. Materials at High Temperatures 2015;32(4):404–12.
[2] Lemaitre J, Chaboche J-L. Mechanics of solid materials. Cambridge university press; 1990.
[3] Dassault Systèmes. Abaqus 6.12 documentation. DS SIMULIA, Providence, Rhode Island 2012.
[4] Armstrong PJ, Frederick CO. A mathematical representation of the multiaxial Bauschinger effect. Central Electricity Generating Board [and] Berkeley Nuclear Laboratories, Research & Development Department; 1966.
[5] Malinin NN, Khadjinsky GM. Theory of creep with anisotropic hardening. International Journal of Mechanical Sciences 1972;14(4):235–46.
[6] Simo JC, Taylor RL. Consistent tangent operators for rate-independent elastoplasticity. Computer Methods in Applied Mechanics and Engineering 1985;48(1):101–18.
[7] Walker AC. A non-linear finite element analysis of shallow circular arches. International Journal of Solids and Structures 1969;5(2):97–107.
[8] Zanger F, Fellmeth A, Gerstenmeyer M, Schulze V. Influence of Kinematic Hardening During machining of ARMCO Iron. 15th CIRP Conference on Modelling of Machining Operations (15th CMMO) 2015;31(0):106–11.
[9] Ibrahim N, Embury JD. The Bauschinger effect in single phase b.c.c. materials. Materials Science and Engineering 1975;19(1):147–9.
[10] Troiano E, Parker AP, Underwood J, Mossey C. Experimental data, numerical fit and fatigue life calculations relating to the Bauschinger effect in high strength armament steels. Journal of pressure vessel technology 2003;125(3):330–4.
[11] Zemzemi F, Rech J, Ben Salem W, Dogui A, Kapsa P. Identification of a friction model at tool/chip/workpiece interfaces in dry machining of 5AISI41426 treated steels. Journal of Materials Processing Technology 2009;209(8):3978–90.
[12] Schulze V, Autenrieth H, Deuchert M, Weule H. Investigation of surface near residual stress states after micro-cutting by finite element simulation. CIRP Annals - Manufacturing Technology 2010;59(1):117–20.
[13] Schulze V, Osterried J, Meier H, Zanger F. Simulation of Multiple Chip Formation when Broaching SAE 5120 Low Alloy Steel 2011;223.
[14] Weber M, Hochrainer T, Gumbsch P, Autenrieth H, Delonnoy L, Schulze V et al. Investigation Of Size-Effects In Machining With Geometrically Defined Cutting Edges. Machining Science and Technology 2007;11(4):447–73.